HIPPOCAMPUS 12:218–234 (2002)
DOI 10.1002/hipo.1110

Three Classes of Pyramidal Neurons in Layer V of Rat Perirhinal Cortex

James R. Moyer, Jr.,[1*] Ewan C. McNay,[1] and Thomas H. Brown[1–3]

[1]*Department of Psychology, Yale University, New Haven, Connecticut*
[2]*Department of Cellular and Molecular Physiology, Yale University, New Haven, Connecticut*
[3]*Interdepartmental Neuroscience Program, Yale University, New Haven, Connecticut*

ABSTRACT: Whole-cell recordings from 140 pyramidal neurons in layer V of rat perirhinal cortex (PR) revealed three distinct firing patterns: regular spiking (RS, 76%), burst spiking (BS, 9%), and late spiking (LS, 14%). LS neurons have not previously been reported in layer V of any cortical region. LS cells in layer V of PR exhibited delays of up to 12 s from onset of a depolarizing current step to spike threshold, followed by sustained firing. In contrast, pyramidal cells in layer V of other cortical regions contain only RS and BS cells. Within PR, the percentage of LS neurons in layer V differs markedly from what we previously observed in layers II/III (50% LS) and VI (90% LS). Morphologically, BS neurons in layer V of PR had thick primary apical dendrites that terminated in a tuft within layer I, whereas RS and LS cells had relatively thin primary apicals that terminated either diffusely or in a layer I tuft. At holding potentials near rest, PR neurons exhibited small (~15 pA), inward, spontaneous postsynaptic currents (PSCs) that were indistinguishable among the three cell types. Currents evoked by minimal stimulation of layer I were about 2.8 times larger than the spontaneous PSCs. Evoked currents had unusually long onset latencies with little variation in latency, consistent with monosynaptic responses evoked by stimulation of unmyelinated fibers. The prevalence of LS cells in combination with the long-latency monosynaptically evoked PSCs suggested that PR is not a region of rapid throughput. This is consistent with anatomical data suggesting that PR is a higher-level association cortex. These data further advance an emerging picture of PR as a cortical region with a unique distribution of cell types different from other cortical regions. ***Hippocampus 2002;12:218–234.*** **© 2002 Wiley-Liss, Inc.**

KEY WORDS: regular spiking; burst spiking; late spiking; brain slices; whole-cell; voltage-clamp; EPSC; evoked current; morphology; parahippocampal

INTRODUCTION

Perirhinal cortex (PR) is important not only because of its role in learning and memory (Suzuki et al., 1993; Zola-Morgan et al., 1993; Herzog and Otto, 1997; Eacott, 1998), but also because it is one of the earliest regions damaged in Alzheimer's disease (Van Hoesen and Solodkin, 1994; deToledo-Morrell et al., 1997; Juottonen et al., 1998). PR has extensive reciprocal connections with the amygdala (Pitkänen et al., 2000), and it serves as a major gateway to the hippocampus through both direct and indirect projections (Burwell et al., 1995; Naber et al., 1999; Suzuki and Eichenbaum, 2000).

Lesion studies in human and nonhuman primates have demonstrated the importance of perirhinal cortex for recognition memory at long intervals. Patients with damage to PR correctly matched complex objects when the delay interval was less than 2 s, but not when the delay was greater than 6 s (Buffalo et al., 1998). In nonhuman primates, PR lesions result in profound deficits in delayed nonmatch-to-sample (DNMS) tasks, particularly at longer delay intervals (Meunier et al., 1993). In rats, damage to PR impairs memory of an odor-guided DNMS task, especially at long delays, analogous to observations in primates (Otto and Eichenbaum, 1992). Perirhinal cortex lesions in rats also result in profound deficits in odor-guided fear conditioning, a DNMS version of an eight-arm maze, water maze, and delayed nonmatch-to-position tasks (Mumby and Pinel, 1994; Herzog and Otto, 1997; Otto et al., 1997; Liu and Bilkey, 1998a,b; Wiig and Burwell, 1998). Taken together, these data suggest that PR is important for temporal aspects of information processing, independent of sensory modality.

Grant sponsor: NIH; Grant numbers: RO1 48660 and RO1 50948; Grant sponsor: NINDS; Grant number: F32 NS09992.
*Correspondence to: Dr. James R. Moyer, Jr., Department of Psychology, P.O. Box 208205, Yale University, New Haven, CT 06520.
E-mail: james.moyer@yale.edu
Accepted for publication 13 June 2001

While there are a large number of lesion studies demonstrating the importance of perirhinal cortex in various learning and memory tasks, little is known about how neurons in perirhinal are organized or how their firing and network properties change during learning. Extracellular single-unit recordings in behaving monkeys suggest that perirhinal neurons respond more to an object when it is novel than to when it is familiar, supporting involvement of perirhinal neurons in recognition memory (Fahy et al., 1993). Similarly, some rat perirhinal neurons fire tonically during the delay period of an odor-guided DNMS task, suggesting that perirhinal neurons may be involved in maintaining a sensory representation of the sample cue during the recognition memory task (Young et al., 1997).

Through comparative studies it is important to understand how neuronal firing properties vary among and within cortical regions (Connors and Gutnick, 1990). To understand better the cellular neurobiology of perirhinal cortex, we have been examining the electrophysiology and morphology of neurons within each of the individual layers. Our previous studies demonstrated that, *unlike any other cortical region*, 50% of the pyramidal neurons in layers II/III (Beggs et al., 2000) and 90% of the large principal neurons in layer VI (McGann et al., 2001) are late-spiking (LS) cells. The present study used visually guided, whole-cell recordings to examine the properties of pyramidal neurons in layer V of rat perirhinal cortex. Our data demonstrate that PR layer V is quite different from its adjacent layers (II/III and VI). Layer V of PR is also unique among cortical regions because it contains three distinct classes of pyramidal cells (RS, BS, and LS). Portions of these data have been presented in abstract form (Moyer and Brown, 1996, 1999; Moyer et al., 1998).

MATERIALS AND METHODS

Slice Preparation

Horizontal brain slices through perirhinal cortex were prepared as previously described (Moyer and Brown, 1998). Sprague-Dawley rats (mean age, 5.2 ± 1.2 weeks) were deeply anesthetized using halothane and decapitated. The brain was quickly removed and placed in ice-cold oxygenated sucrose-CSF (composition in mM: 206 sucrose, 2.8 KCl, 1 $CaCl_2$, 1 $MgCl_2$, 2 $MgSO_4$, 1.25 NaH_2PO_4, 26 $NaHCO_3$, and 10 D-glucose) for about 3 min. The brain was then blocked, hemisected, and glued to the tray of a vibratome (ventral surface up). Horizontal brain slices (300–400 μm) were cut at ~1°C, using a temperature-controlled vibratome. Slices were removed and placed into individual wells of our 24-well slice incubation chamber (Moyer and Brown, 1998). The chamber contained oxygenated artificial CSF (aCSF; composition in mM: 124 NaCl, 2.8 KCl, 2 $CaCl_2$, 2 $MgSO_4$, 1.25 NaH_2PO_4, 26 $NaHCO_3$, and 10 D-glucose, pH 7.4, 295 mOsmol). Slices were allowed to recover at room temperature (23–25°C) for at least 1 h prior to beginning any experiment. Cutting and recording solutions used in earlier experiments contained 2.0 mM KCl rather than 2.8 mM KCl. No differences in cell properties were observed and data were pooled.

Visualization of Neurons and Whole-Cell Recordings

An upright microscope (Zeiss Axioskop) equipped with a 40× water immersion objective (0.75 NA), infrared filtered light, DIC optics, and a Hamamatsu C2400 video camera and video enhancement device was used for visualization of the cell and patch electrode (Keenan et al., 1988; Moyer and Brown, 1998; Xiang and Brown, 1998). Video images were captured on a PC using Bio-Rad's COMOS software in video-capture mode and transferred to a Macintosh computer using NIH Image. PR was defined according to previously published coordinates (Burwell et al., 1995; Burwell and Amaral, 1998). Only slices corresponding to plates 98–100 of a rat stereotaxic atlas (Paxinos and Watson, 1998) were used. Recordings were restricted to the rostrocaudal area of −3.8 to −5.2 mm relative to bregma.

Whole-cell recordings were made from 140 visually identified pyramidal neurons from layer V of rat perirhinal cortex using either an AxoPatch 1D or 200A amplifier (Axon Instruments, Foster City, CA), as previously described (Moyer and Brown, 1998). Cells were located an average of 70.8 ± 1.5 μm below the slice surface (range, 30–135 μm). Cells were classified as RS, BS, and LS based on their discharge patterns (described in detail in Results). Only cells with a stable uncorrected resting membrane potential more negative than −60 mV and overshooting action potentials of at least 70 mV (measured from threshold) were analyzed. All recordings were somatic. Therefore, references to transmembrane potentials only apply to the soma; we do not assume that the cells are isopotential. Patch pipettes (mean resistance: 3.7 ± 0.1 MΩ) were fabricated from borosilicate glass (i.d. 1.303 mm, o.d. 1.689 mm; Drummond Scientific) using a Sutter Instruments model P-97 puller. Pipettes were filled with the following solution (in mM): 110 K-gluconate, 10 HEPES, 1.0 EGTA, 20 KCl, 2.0 $MgCl_2$, 2.0 Na_2ATP, 0.25 Na_3GTP, and 10 phosphocreatine (di-tris), pH 7.3, 290 mOsmol. In most experiments, electrodes also contained 0.5% biocytin to obtain cellular morphology (Moyer et al., 1998; Faulkner and Brown, 1999). In some experiments, pipette tips were fire-polished and/or coated with Sylgard to reduce capacitance noise.

Voltages were corrected for a measured +13 mV liquid junction potential between the bath and patch pipette solutions, according to the equation $V_M = V_P - V_L$, where V_M is the corrected membrane voltage, V_P is the observed pipette voltage and V_L is the liquid-liquid junction potential (Moyer and Brown, 1998). A bipolar concentric electrode was used for synaptic stimulation of layer I afferents. Signals were filtered at 2 kHz, digitized at 44 kHz, and stored on VCR tape for off-line analysis using custom software written for IgorPro (WaveMetrics, Lake Oswego, OR). The individual evoked current sweeps shown in Figure 10A,B were digitally filtered within IgorPro using a binomial algorithm (Marchand and Marmet, 1983), with a smoothing parameter of 3. Tetrodotoxin, bicuculline methobromide, and picrotoxin were purchased from Sigma (St. Louis, MO), and 6-cyano-7-nitroquinoxaline-2,3-di-

one (CNQX) and DL-2-amino-5-phosphonovalerate (APV) were purchased from Tocris (Ballwin, MO).

Morphological Reconstructions of Layer V Pyramidal Neurons

Reconstructions were obtained from 77 biocytin-filled layer V pyramidal neurons. Without exception, neurons that were deemed pyramidal under IR-DIC visualization were also confirmed morphologically to be pyramidal. Reconstructions were obtained as previously described (Faulkner and Brown, 1999). After recording, slices were incubated in 4% paraformaldehyde/0.1 M phosphate-buffered saline (PBS) at least overnight at 4°C, followed by 30% sucrose/PBS for 24–48 h. Thin sections (50–65 μm) were cut on a freezing microtome and collected as free-floating slices in PBS. Sections were then incubated in avidin and biotinylated horseradish peroxidase (HRP), using the VectaStain Elite ABC kit (Vector Laboratories, Burlingame, CA) following the manufacturer's instructions, and HRP was localized using diaminobenzidine tetrahydrochloride (DAB). Slices were then incubated in ascending concentrations of glycerol (20–100%) and mounted in 100% glycerol. Sections were then coverslipped, and the coverslip was sealed with nail polish. Individual neurons were reconstructed using a camera lucida drawing tube attached to a Zeiss Axioskop. Cells were reconstructed using either a 40× air objective (0.85 NA and an air condenser) or 63× oil objective (1.4 NA and an oil condenser).

Data Analysis and Statistics

Gigaohm seal resistance was calculated in response to a 25 mV hyperpolarizing voltage step (mean resistance, 5.7 ± 0.4 GΩ). Whole-cell capacitance (mean, 8.6 ± 0.2 pF) and series resistance (mean, 7.3 ± 0.6 MΩ) were estimated from dials on the AxoPatch 1D amplifier after compensation for capacitance transients. In all current-clamp experiments, 800-ms or 5,000-ms alternating hyperpolarizing and depolarizing current steps were used to evaluate cellular membrane properties. In experiments with LS neurons, longer duration steps (10, 20, or 40 s) were occasionally used to evaluate their responses to suprathreshold current injections. Voltage-current (V-I) relations were constructed for all neurons.

Neuronal input resistance (R_N) was calculated from the slope of the line (least-squares regression) in the linear portion of the V-I relationship, near the resting potential, where alternating hyperpolarizing and depolarizing voltage responses were symmetrical. Measurements of R_N were made at two different times: early (50 ms after current onset) and late (50 ms prior to current offset). Since the late measurement was taken at steady-state, well beyond the time constant (τ_m) of the membrane voltage response, it is used in the text as the neuronal input resistance. The early measurement was only taken to check for the presence of fast active conductances. Individual current injections (<20 pA) that resulted in small voltage deflections (<10 mV), well within the linear portion of the V-I relationship, were used to obtain estimates of τ_m.

The current required to elicit a single AP was determined by increasing the depolarizing current amplitude in 5 pA increments until a spike was elicited and then finding threshold using iterations of ±1–2 pA. The AP amplitude was calculated from threshold, and the width was calculated at one-half the amplitude. AHPs were measured after the first AP elicited by current injections less than 50 pA above threshold. The amplitude and duration of these single-spike AHPs were measured relative to spike threshold. Typically, BS cells lacked a measurable AHP after the first AP (11 of 13 cells). In these cases, BS cells were given a value of zero for both the amplitude and duration of the first-spike AHP. To characterize further the firing properties of each of the three cell types, the interspike interval (ISI) between each spike during a spike train was plotted against the interval number at different stimulus intensities (ISI-interval number plots).

Spontaneous postsynaptic currents (PSCs) were measured for 2–6 min at the resting potential and at several different holding potentials (range, −95 to −55 mV). Detection of spontaneous PSCs involved the use of an autodetection program written in IgorPro, followed by visual inspection of all detected currents. Only currents that were at least three times larger than the RMS noise (~1.4 pA) were included. The number and frequency of spontaneous PSCs were calculated. For individual PSCs, the 10/90 and 20/80 rise times, the decay constant, and the peak amplitude were calculated, and the data were averaged for each cell.

For experiments with TTX, data were analyzed after bath application of TTX for 20–30 min. The effectiveness of TTX was confirmed by a complete block of synaptically evoked responses, which generally occurred within 4 min. Cumulative probability distributions were constructed to evaluate the effects of TTX on spontaneous PSC amplitudes. Amplitude data were binned at 2 pA intervals, and the cumulative frequency was divided by the total number of events to obtain the cumulative probability distribution. Cumulative probability distributions were compared using the Kolmogorov-Smirnov (K-S) test applied to unbinned cumulative probability distributions to evaluate significant effects of TTX.

Synaptic currents were evoked by stimulating layer I, using a concentric bipolar platinum electrode (FHC, Bowdoinham, ME) at minimal or near-minimal stimulation (we attempted to find a stimulation intensity just above threshold). We use the term "near-minimal" to distinguish it from the more rigorous minimal stimulation typically used in quantal analysis studies to prove that only one afferent is stimulated (Xiang and Brown, 1998). Only cells with evoked currents that displayed little variability in onset latency were studied. In some cases, the stimulating electrode was moved several times within layer I to obtain what appeared to be a monosynaptic response. Latency to onset, rise time, decay time, and peak amplitude were calculated for each evoked response and averaged for each cell. The coefficient of variation of the onset latency was also calculated. For evoked and spontaneous PSCs, I-V plots were constructed by taking peak amplitude measurements of the current at several different holding potentials. A least-squares linear regression fit through the I-V plot was used to estimate the slope conductance.

Statistical analyses were performed using a commercial software package (Statview, Abacus Concepts). One-way analysis of variance (ANOVA) was used to evaluate group effects (RS, BS, and LS), and paired *t*-tests were used to evaluate drug effects (aCSF,

TABLE 1.

Comparisons Between Pyramidal Cell Classes in Layer V of Rat Perirhinal Cortex[a]

Cellular property measured	Cell Classification (*n*)		
	Regular spiking	Burst spiking	Late spiking
Resting membrane potential (mV)	−77.4 ± 0.3 (107)	−77.2 ± 1.4 (13)	−77.6 ± 0.7 (20)
Input resistance, early (MΩ)	161.2 ± 5.0 (104)	141.5 ± 11.2 (13)	194.9 ± 11.5 (20)*
Input resistance, late (MΩ)	257.4 ± 11.9 (107)	205.5 ± 34.5 (13)*	312.7 ± 22.5 (20)*
Time constant (ms)	66.4 ± 2.3 (104)	59.1 ± 7.6 (13)	72.7 ± 5.0 (20)
Spike threshold (mV)	−53.7 ± 0.4 (104)	−56.5 ± 2.2 (13)*	−52.6 ± 0.9 (20)
Action potential amplitude (mV)	94.0 ± 0.9 (107)	97.9 ± 2.3 (13)	90.9 ± 1.8 (20)
Action potential width (ms)	2.0 ± 0.04 (104)	1.8 ± 0.09 (13)*	2.2 ± 0.11 (20)
Action potential rise:fall dV/dt ratio	3.6 ± 0.1 (104)	3.2 ± 0.3 (13)	3.7 ± 0.3 (20)
Single spike AHP amplitude (mV)	8.4 ± 0.3 (104)**	0.5 ± 0.4 (13)**	12.5 ± 0.6 (20)**
Single spike AHP duration (ms)	276.1 ± 17.8 (104)**	16.5 ± 5.8 (13)**	473.8 ± 76.8 (20)**
Mean rat age (weeks)	5.2 ± 1.4 (107)	5.7 ± 2.0 (13)	4.8 ± 2.4 (20)

[a]One-way ANOVA revealed a statistically significant main effect of cell type on input resistance, early ($F_{2,134} = 5.34$, $P < 0.005$); input resistance, late ($F_{2,137} = 3.28$, $P < 0.05$); spike threshold ($F_{2,134} = 3.37$, $P < 0.05$); action potential width ($F_{2,134} = 4.14$, $P < 0.05$); single-spike AHP amplitude ($F_{2,134} = 66.05$, $P < 0.001$); and single-spike AHP duration ($F_{2,134} = 19.72$, $P < 0.001$) among the three cell classes. Post hoc comparisons made using Fisher's PLSD: input resistance, early (LS-BS and LS-RS *$P < 0.05$); input resistance, late (BS-LS *$P < 0.05$); spike threshold (BS-RS and BS-LS *$P < 0.05$); action potential width (BS-RS and BS-LS *$P < 0.05$); single-spike AHP amplitude and duration (all groups significantly different from each other, **$P < 0.001$).

TTX). If the ANOVA was significant (0.05 level), a Fisher's PLSD was used for post hoc comparisons. All data are reported as the mean ± standard error of the mean.

RESULTS

Layer V pyramidal cells had a mean resting membrane potential (E_R) of −77.4 ± 0.2 mV, an input resistance (R_N) of 260.5 ± 10.3 MΩ, a time constant (τ_m) of 66.6 ± 2.0 ms, and an action potential amplitude (AP_{amp}) of 93.9 ± 0.8 mV. A mean current injection of +60.7 ± 3.6 pA was required to elicit an AP, and the average threshold voltage for AP generation was −53.8 ± 0.4 mV. All 140 neurons fit into one of three classifications, as described below.

Physiology and Morphology of Regular Spiking Pyramidal Neurons in Layer V of Rat Perirhinal Cortex

Most layer V pyramidal cells (107 of 140) were RS adapting neurons (Table 1). Figure 1A illustrates that the pyramidal somata were easily identified using IR-DIC optics; this was true for all three cell types and was also confirmed by all 77 reconstructions. The voltage-current relation (V-I relation) was linear at 50 ms, indicating the absence of any fast active conductances (Fig. 1A, triangles), but showed inward rectification at 750 ms (Fig. 1A, circles). A sag in the voltage response was present in response to large hyperpolarizing current injections (Fig. 1A, asterisk) and was typical of RS cells (103 of 107 cells). In response to suprathreshold current injections, RS cells fired their first AP shortly after onset of the current pulse. With larger current injections, the interspike interval (ISI) between APs increased across time (Fig. 1B), similar to RS adapting cells in other cortical regions (McCormick et al., 1985; Schwindt et al., 1997). Frequency adaptation is clearly visualized by the upward shape of the family of ISI-interval number curves (Fig. 2A). A graph of the first ISI as a function of current injection reveals the rapid decrease in first ISI as more current is injected into the soma (Fig. 2A, inset, solid symbols).

Within layer V, RS pyramidal cells were located both in upper (Va, n = 51) and lower (Vb, n = 56) regions. Morphologically, they have prominent basilar dendrites and a thin primary apical dendrite (some bifurcating) that terminated either diffusely or in a tuft within layer I. Examples of the range of RS morphologies observed are shown in Figure 3. All 54 reconstructed RS cells possessed numerous spines throughout both the basilar and apical dendrites, including the primary apical. Axons of RS cells tended to ramify within layer V and project toward layer VI and the external capsule (data not shown).

Physiology and Morphology of Burst-Spiking Pyramidal Neurons in Layer V of Rat Perirhinal Cortex

Burst-spiking (BS) cells generated an initial burst of 2–4 APs in response to a just-suprathreshold depolarizing current step or syn-

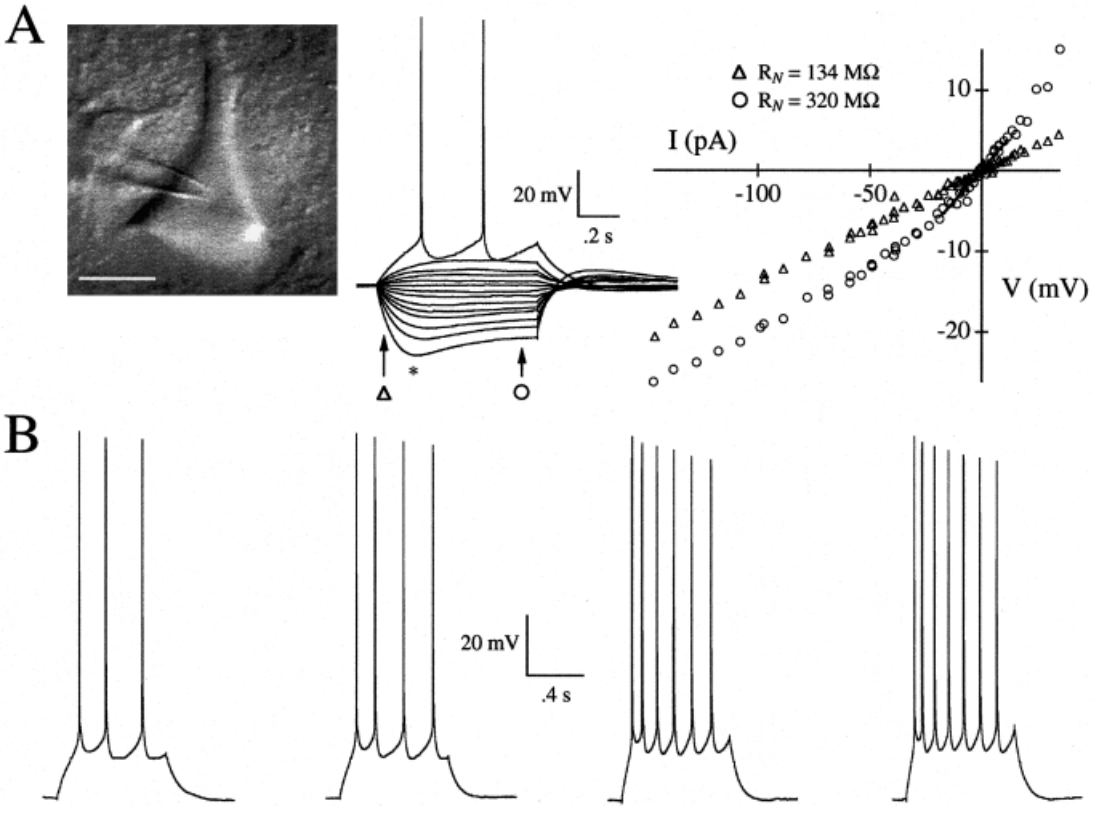

FIGURE 1. Intrinsic properties of regular spiking pyramidal neurons in layer V of rat perirhinal cortex. A: At left, a video image shows the position of the patch pipette on the soma (scale bar, 10 μm; pial surface up). At center is an overlay of voltage traces in response to hyperpolarizing and depolarizing current injections in the same RS cell (E_R = −78 mV; R_N = 320 MΩ; AP_{amp} = 97 mV). Notice the pronounced sag (onset denoted by asterisk) in the voltage response to hyperpolarizing current injections characteristic of RS cells. At right is the voltage-current (V-I) relation for this cell. Open triangles and open circles represent measurements taken at 50 ms and 750 ms after onset of current pulse (see arrows in middle image). The V-I relation measured at 750 ms shows inward rectification, while that at 50 ms is linear, indicating the absence of fast active conductances. B: Responses of another RS cell (E_R = −78 mV; R_N = 403 MΩ; AP_{amp} = 102 mV) to increasingly larger depolarizing current injections (from left to right: +30 pA, +39 pA, + 59 pA, +69 pA). In response to suprathreshold depolarizing current injections, RS cells fire APs early during the step. Note that with larger current injections, more APs are elicited, and that the interval between spikes increases across time (frequency adaptation).

aptic stimulation. Burst spiking was observed in 13 of 140 PR layer V pyramidal neurons. As with previous studies in rat sensorimotor and visual cortices (Franceschetti et al., 1993; Kasper et al., 1994b), we only observed burst spiking in cells from animals ≥14 days of age. Table 1 summarizes and compares the electrophysiological properties of BS pyramidal cells with those of RS and LS cells in layer V of rat PR. A typical feature of BS cells was the lack of an AHP following the first AP. Only two BS cells had a measurable AHP after the first spike, while in the other 11 BS cells, the second spike within the burst occurred before the membrane voltage returned to the threshold voltage for elicitation of the first AP. Figure 4A shows a typical BS cell that fired a burst of three APs in response to a just-suprathreshold depolarizing current step. Notice that subsequent spikes in the burst are smaller than the initial spike, as was true of all BS neurons, possibly due to prolonged sodium channel inactivation (Jung et al., 1997; Williams and Stuart, 1999).

Like RS neurons, the V-I relation of BS cells was linear at 50 ms (Fig. 4A, triangles) and showed inward rectification at 750 ms after current onset (Fig. 4A, circles). A sag in the voltage response to hyperpolarizing current injections was also typical (12 of 13 cells) of BS neurons (Fig. 4A, asterisk). BS cells always fired an initial burst of 2–4 action potentials, followed by either a second burst or a series of single adapting APs (Fig. 4B), similar to those seen in low-threshold BS cells previously reported in rat sensorimotor cortex (Schwindt et al., 1997). ISI-interval number plots of BS cells reveal that curves generated at different stimulus intensities all emerge from a nearly identical initial ISI (Fig. 2B, interval number 1). Indeed, the lack of variation in the initial ISI, plotted as a function of injected current, was characteristic of BS cells (Fig. 2B, inset, solid symbols).

BS pyramidal cells were located both in upper (Va, n = 5) and lower (Vb, n = 8) regions of layer V. Morphologically, BS cells had variable amounts of basilar and oblique dendrites emerging from the soma, and they displayed a thick, nontapering primary apical dendrite that terminated in a tuft within layer I. Examples of typical BS cell morphologies are shown in Figure 5. Like the BS pyramidal cells described in layer V of somatosensory and visual cortices (Chagnac-Amitai et al., 1990; Kasper et al., 1994a), the thick, nontapering

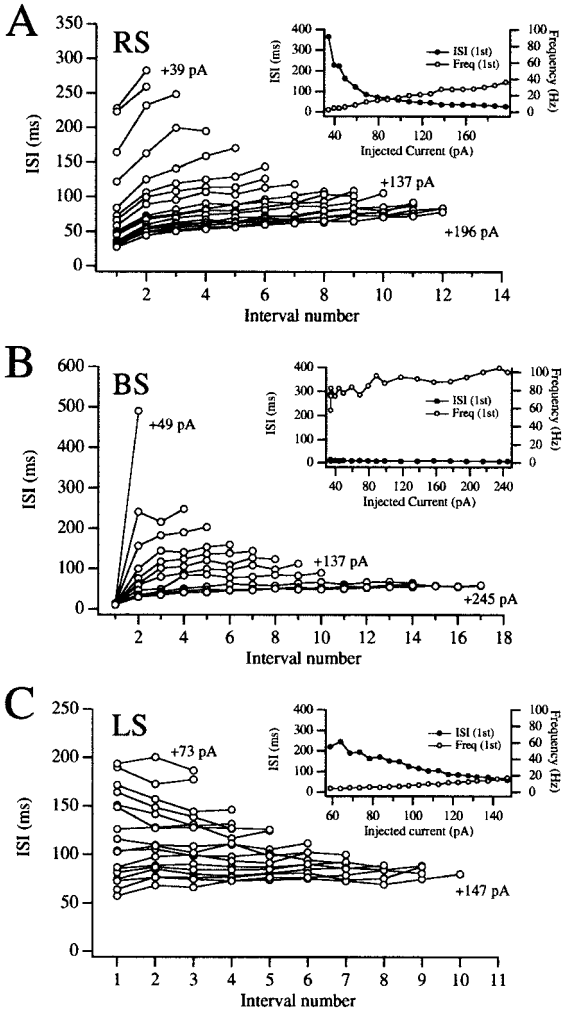

FIGURE 2. Plots of interspike interval (ISI) vs. interval number in the three classes of perirhinal layer V pyramidal cells. A: With larger depolarizing current injections, RS cells show a decrease in initial ISI, while continuing to show adaptation. Inset: Initial ISI and firing frequency plotted as a function of injected current. The first ISI rapidly decreases with larger current injections (solid circles). This cell was capable of generating an initial firing frequency of 40 Hz (open circles). B: ISI-interval number plots of BS cells indicate that the interval between the first two APs is consistent and independent of size of the depolarizing current injection. Subsequent intervals increase in duration (adaptation), even with extremely large current injections (e.g., +245 pA). Inset clearly shows that the initial ISI changed little as a function of current injection (solid circles), and that this cell could achieve an initial firing frequency of about 100 Hz (open circles). C: ISI-interval number plots of LS cells indicate that small current injections result in a progressive decrease in ISI as a function of interval number (anti-adaptation), whereas larger current injections (in this case, 120–147 pA) result in a progressive increase in ISI across intervals (frequency adaptation). Inset shows that the initial ISI decreases steadily as a function of current injection (solid circles) and that an initial firing frequency of <20 Hz was achieved (open circles).

primary apical dendrite was characteristic of BS pyramidal neurons in layer V of rat PR. All nine reconstructed BS cells had a thick primary apical dendrite and possessed numerous spines throughout both the basilar and apical dendrites (including the primary apical). Axons of BS cells tended to ramify within layer V and project toward the external capsule (data not shown).

Physiology and Morphology of Late-Spiking Pyramidal Neurons in Layer V of Rat Perirhinal Cortex

Late spiking (LS) was the most surprising firing pattern observed among perirhinal layer V pyramidal neurons (20 of 140). Late-spiking cells have not been reported in layer V of any other cortical region. Unlike RS and BS cells, which fired shortly after onset of a just-suprathreshold depolarizing current injection, LS neurons exhibited an initial rapid rise in membrane voltage followed by a slowly ramping depolarization that led to an AP near the end of a just-suprathreshold current step. Electrophysiological characteristics of the 20 LS neurons and comparisons with RS and BS cells are presented in Table 1. In response to hyperpolarizing current injections, the V-I relation of LS cells was linear at 50 ms (Fig. 6A, triangles) and showed inward rectification at 750 ms (Fig. 6A, circles), like RS and BS cells. Note the relative absence of a sag in the hyperpolarizing voltage responses, and the presence of a slow depolarizing ramp prior to the first action potential near the end of the current step (Fig. 6A, curved arrow). The absence of an obvious sag in the voltage response was typical of LS neurons, unlike RS and BS cells (compare with Figs. 1 and 4).

Examples of the exceptionally long delays typical of LS neurons in layer V are shown in Figure 6B. When long steps of 10–40 s were used, spike delays between 7–12 s were common (Fig. 6B, top traces). In each case the long delays were also followed by sustained firing throughout the current step, even in response to a 40-s, +38-pA current injection (Fig. 6B, bottom trace). Early in the spike train the intervals between APs remained fairly constant or decreased, while spike intervals later in the train tended to increase (Fig. 6B, top right trace and bottom trace). Unlike either RS or BS cells, the ISI-interval number plots of LS cells typically showed anti-adaptation at small stimulus intensities, followed by mild adaptation at larger stimulus intensities (Fig. 2C). The initial ISI vs. injected current plot of LS cells illustrates that the first ISI decreases fairly linearly with increasing current (Fig. 2C, inset).

LS pyramidal cells were located in both upper (Va, n = 9) and lower (Vb, n = 11) regions of layer V. Morphologically, LS cells had prominent basilar dendrites and thin primary apicals (some bifurcating) that terminated either diffusely within layer V or in a tuft within layer I (Fig. 7). All 14 reconstructed LS neurons possessed numerous spines throughout both the basilar and apical dendrites. Axons of LS cells tended to ramify within layers V and VI as well as project up toward layers II/III (data not shown).

Spontaneous Postsynaptic Currents in Perirhinal Layer V Pyramidal Neurons

To date there have been no studies of spontaneous PSCs in layer V of PR. Spontaneous PSCs from 16 layer V pyramidal cells were analyzed in detail at holding potentials near rest (Table 2). No statistically significant differences in the size, shape, and frequency of spontaneous PSCs were observed among the three different cell

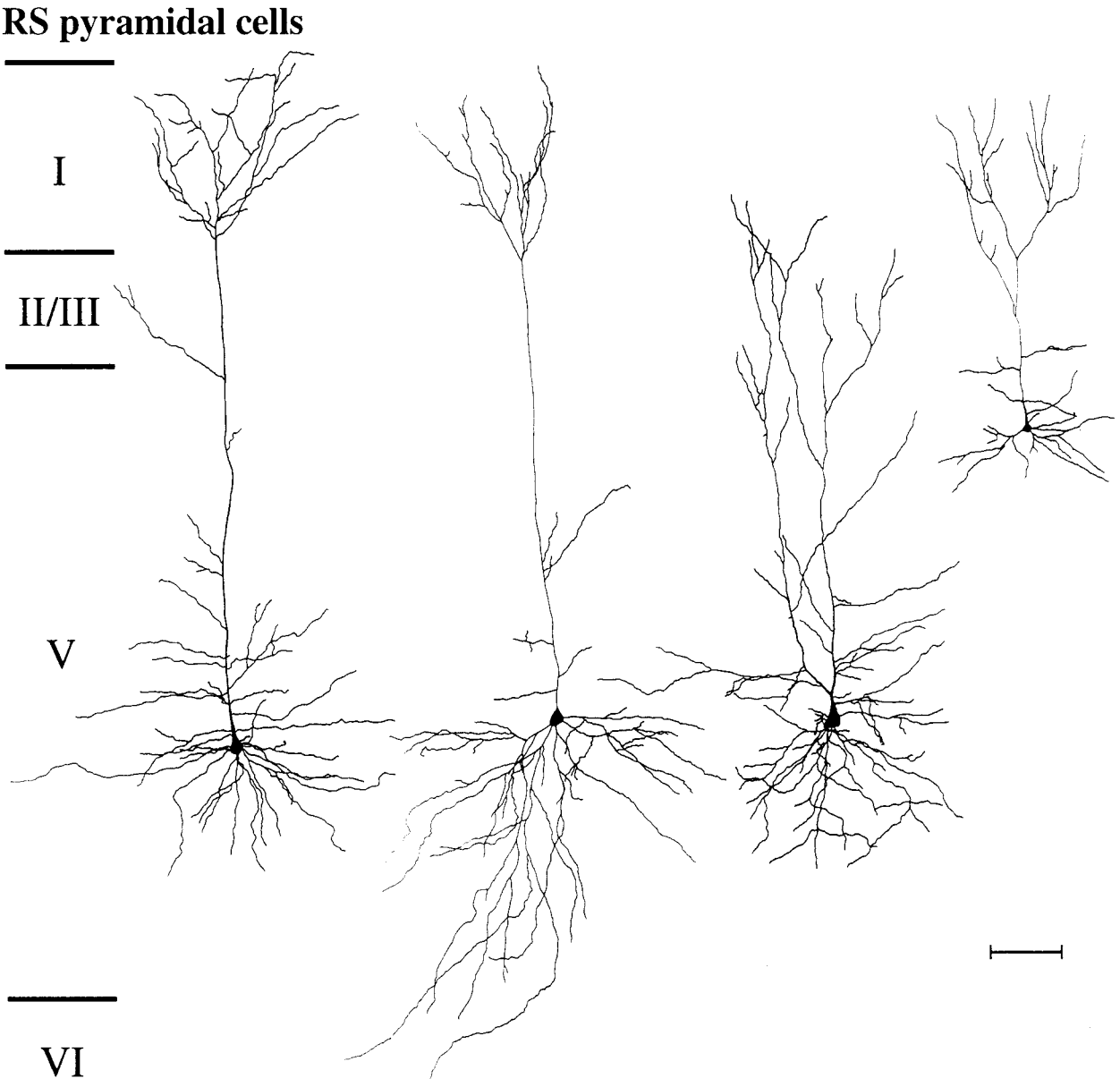

FIGURE 3. Morphology of regular spiking pyramidal neurons in layer V of rat perirhinal cortex. Shown are camera lucida drawings from four biocytin-filled RS cells, indicating the range of morphologies observed (n = 54). Most cells had prominent basilar dendrites and a thin apical dendrite that terminated in a tuft within layers II/III or I (left two cells). One RS cell had thin bifurcating apical dendrites that terminated diffusely within layer II/III (second cell from right). Cells located in upper regions of layer V had thin apical dendrites that terminated in a tuft within layer I (right cell). While spines were not drawn, all cells had numerous spines distributed throughout their basilar and apical dendritic trees. Cortical layers are indicated by bars and roman numerals (Scale bar, 100 μm).

types, so the data were pooled. Spontaneous PSCs in PR are much smaller (~15 pA) than those we see in the adjacent lateral amygdala (Faulkner and Brown, 1999). Inhibitory currents were not analyzed in detail but were observed at holding potentials more depolarized than −50 mV (data not shown).

Spontaneously occurring PSCs may include currents activated by neurotransmitter quanta released either spontaneously or through presynaptic spike activity. To evaluate the origin of spontaneous PSCs in PR layer V pyramidal neurons, spontaneous currents were collected from seven neurons before and after bath application of tetrodotoxin (TTX). TTX reduced the frequency and mean amplitude of spontaneous PSCs (Fig. 8). Under control conditions the amplitude frequency histogram was positively skewed (Fig. 8A, open bars). Bath application of 0.5 μM TTX had little effect on the general shape of the amplitude frequency histogram for events smaller than 20 pA, but it nearly eliminated spontaneous PSCs larger than 20 pA (Fig. 8A, shaded bars, and Fig. 8B). Indeed, the leftward shift of the cumulative probability distribution in TTX reflects a statistically significant amplitude reduction (Fig. 8C, K-S test, $P < 0.001$).

Statistical analyses (paired *t*-tests) indicated that bath application of TTX (n = 7) significantly decreased both the mean ampli-

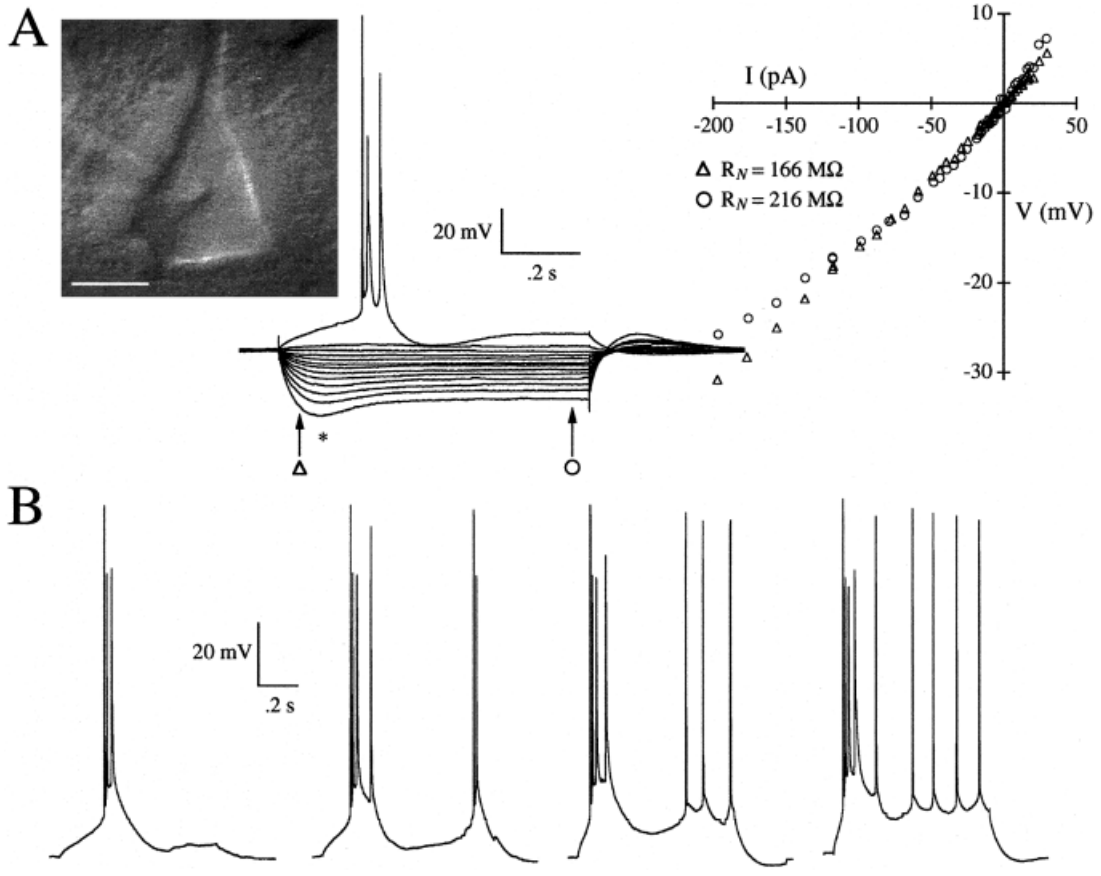

FIGURE 4. Intrinsic properties of burst-spiking pyramidal neurons in layer V of rat perirhinal cortex. A: At left, a video image shows the position of the patch pipette on the cell body (scale bar, 10 μm; pial surface up). Middle image is an overlay of voltage traces in response to hyperpolarizing and depolarizing current injections in the same BS cell (E_R = −78 mV; R_N = 216 MΩ; AP_{amp} = 107 mV). This cell fired a burst of three APs in response to a just-suprathreshold depolarizing current injection (+34 pA). BS cells also showed a prominent sag in the voltage response to hyperpolarizing current injections (onset denoted by asterisk). Right image shows the V-I relation measured at 50 ms (open triangles) and 750 ms (open circles) after current onset. B: Responses of another BS cell (E_R = −76 mV; R_N = 161 MΩ; AP_{amp} = 98 mV) to increasing amounts of depolarizing current injection (from left to right). Initially, one burst of three APs was elicited in this cell after injection of +25 pA (left trace). A current injection of +30 pA resulted in a second burst, but additional increases in current resulted in single adapting APs (right two traces).

tude (15.9 ± 1.7 pA before TTX; 11.2 ± 1.0 pA after TTX; t_6 = 3.33, $P < 0.05$) and frequency (4.0 ± 0.8 Hz before TTX; 1.9 ± 0.5 Hz after TTX; t_6 = 3.74, $P < 0.01$) of spontaneous PSCs without effects on 10/90 rise time ($t_6 = -0.59$, $P > 0.5$), 20/80 rise time ($t_6 = -0.81$, $P > 0.4$), or decay constant ($t_6 = -1.01$, $P > 0.3$). These data are consistent with previous observations of the effects of tetrodotoxin on spontaneous PSCs in other brain regions (Livsey and Vicini, 1992; Arancio et al., 1994; Xiang, 1995; Berretta and Jones, 1996; Cormier and Kelly, 1996; Smith and Dudek, 1996).

To address the identity of the spontaneous PSCs, 50 μM APV and 10 μM CNQX were bath applied to block NMDA and AMPA receptors, respectively (n = 3). Under control conditions, the amplitude frequency histogram was positively skewed (Fig. 9A, open bars). With APV and CNQX present, virtually no spontaneous PSCs were observed (Fig. 9A,B). In the presence of TTX, bath application of a combination of 10 μM bicuculline and 10 μM picrotoxin had no effect on the frequency, amplitude, rise time, or decay time of spontaneous PSCs (n = 2, data not shown). The results indicate that $GABA_A$ currents were not contributing to these histograms and suggest that the spontaneous currents observed at membrane potentials near rest were glutamatergic.

Synaptically Evoked Currents in Perirhinal Layer V Pyramidal Neurons

Evoked PSCs were studied in 25 PR layer V pyramidal neurons (18 RS, 5 BS, and 2 LS). Mean evoked data for layer V cells voltage-clamped near −75 mV are summarized in Table 3. No statistically significant differences were seen among the three cell types, so the data were pooled. Figure 10A shows typical responses to layer I stimulation. In this cell, the mean latency to PSC onset was 11.7 ± 0.1 ms with a coefficient of variation (CV) of 0.05. The small CV is consistent with the possibility that these were monosynaptic PSCs. Currents evoked by near-minimal stimulation of layer I were 2.8 times larger than the mean of all spontaneous currents studied under control conditions. A similar ratio was ob-

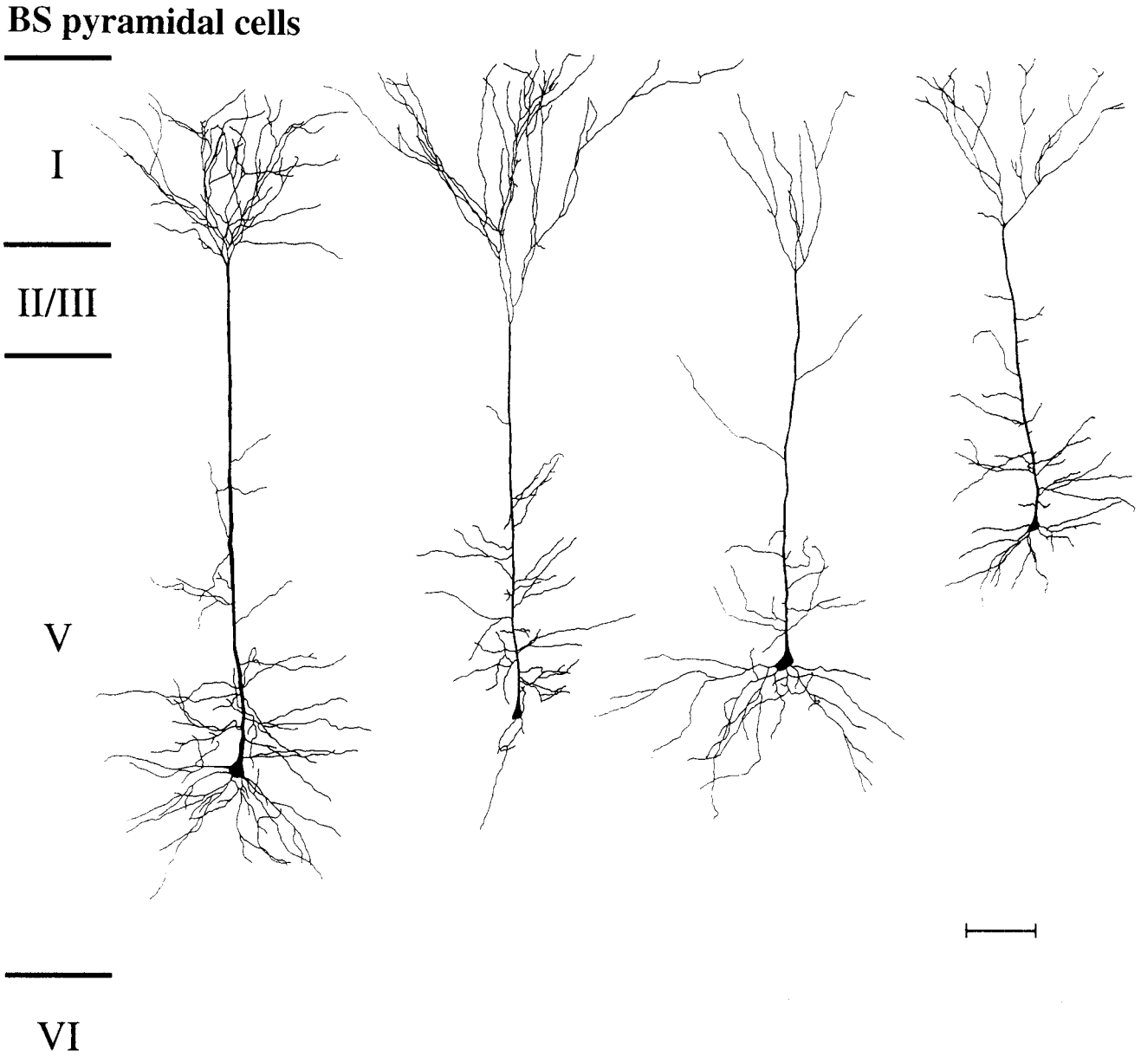

FIGURE 5. Morphology of burst-spiking pyramidal neurons in layer V of rat perirhinal cortex. Reconstructions from four biocytin-filled BS cells illustrate the range of morphologies observed (n = 9). BS cells had variable amounts of basilar and oblique dendrites emerging from the soma, and all were characterized by a *thick* prominent apical dendrite that terminated in a tuft within layer I. Two BS cells were relatively devoid of basilar dendrites, but did have a thick primary apical dendrite ending in a tuft within layer I (second cell from right). BS cells also had numerous secondary dendrites emerging from the apical dendrite prior to the apical tuft. Although not drawn, BS cells had many spines located throughout their basilar and apical dendrites. Cortical layers are indicated by bars and Roman numerals (Scale bar, 100 μm).

served when spontaneous and evoked currents were compared in the same cells (evoked 33.3 ± 7.6 pA, spontaneous 14.7 ± 1.4 pA, n = 9). Electrode distance (distance between stimulating and recording electrodes) was positively correlated (r = 0.8) with onset latency of evoked PSCs. The slope of the linear regression suggested a conduction velocity of ~0.16 m/s (r^2 = 0.6, n = 21), consistent with velocities reported in unmyelinated fibers (Berg-Johnsen and Langmoen, 1992; Murakoshi et al., 1993; Lohmann and Rörig, 1994). Extrapolating the regression line to zero distance suggested a synaptic plus excitation delay of about 1.2 ms.

The relative insensitivity of evoked PSC amplitudes to holding potentials from −90 to −60 mV is indicative of excitatory inputs (Fig. 10C,D). Indeed, this was confirmed by blockade of evoked PSCs by 50 μM APV and 10 μM CNQX (n = 2, data not shown). A least-squares regression fit through the plot of evoked EPSC amplitude plotted against holding current (r^2 = 0.95; Fig. 10C) indicated a slope conductance of 454 pS (data not shown). Note that the evoked currents shown in Figure 10C also contained a late outward component, presumably GABAergic. This slow outward component was rarely observed

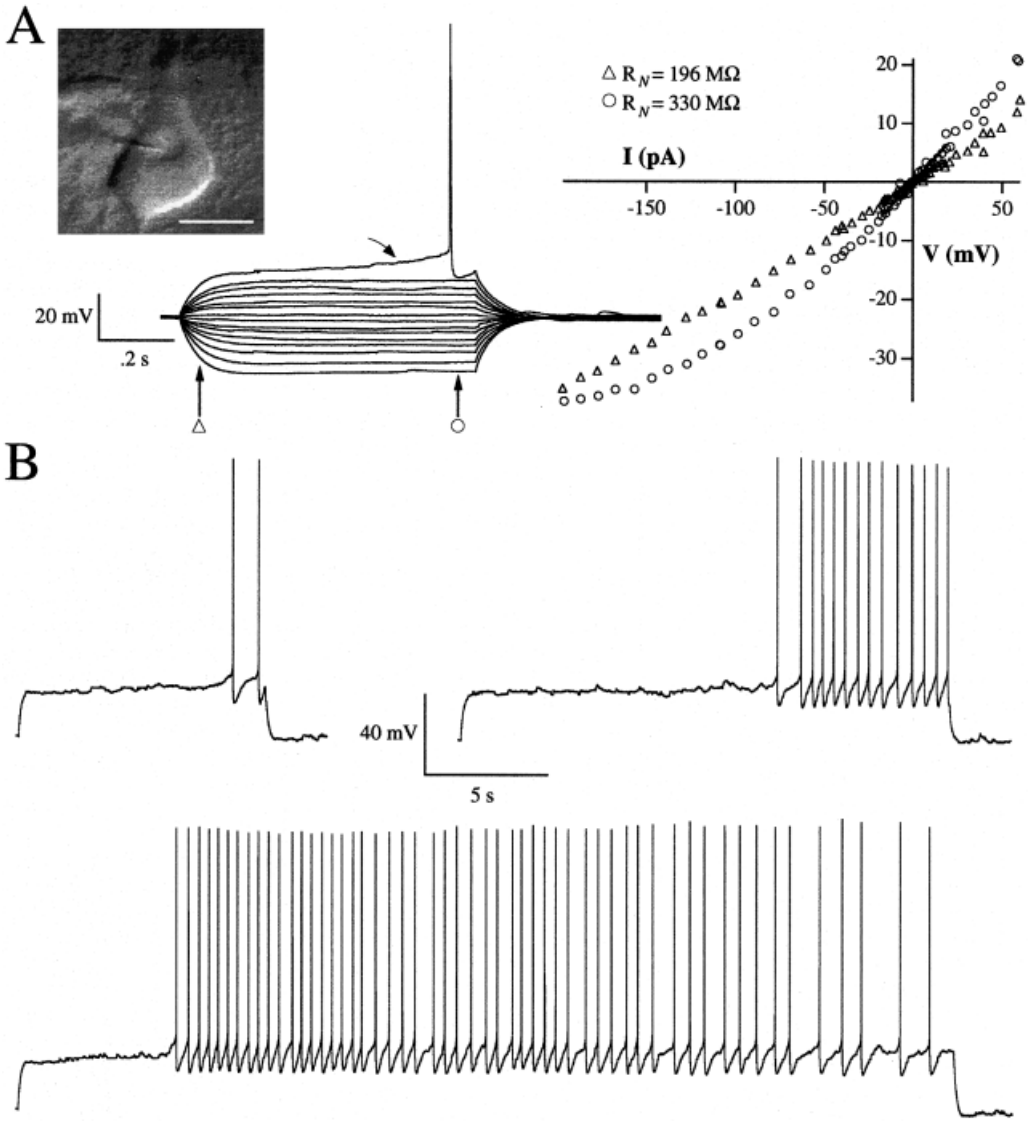

FIGURE 6. Intrinsic properties of late-spiking pyramidal neurons in layer V of rat perirhinal cortex. A: At left, a video image shows the position of the patch pipette on the soma (scale bar, 10 μm; pial surface up). Middle image is an overlay of voltage traces in response to hyperpolarizing and depolarizing current steps in the same LS cell (E_R = −84 mV; R_N = 330 MΩ; AP_{amp} = 98 mV). Note the depolarizing ramp preceding initiation of the first AP near the end of the current step (curved arrow). Note also the absence of a sag in the voltage response to hyperpolarizing current injections. At right is the V-I relation measured at 50 ms (open triangles) and 750 ms (open circles) after the current step. B: LS cells respond to long current steps with unusually long delays prior to spiking. Upper left trace shows voltage response to a 10 s, +39 pA current step. The membrane voltage exhibits a steady ramp depolarization until threshold is reached and the cell fires its first AP ~7.5 s later. Upper right trace shows the response to a 20 s, +37 pA current step resulting in a 12 s delay and sustained firing. Lower trace clearly indicates the ability of LS cells to show both long delays before spiking (~7 s) and sustained firing throughout the pulse (40 s, +38 pA). Note that LS neurons show anti-adaptation early in the spike train and adaptation later in the spike train. Voltage traces in B are from the same cell (E_R = −79 mV; R_N = 434 MΩ; AP_{amp} = 100 mV).

and was not analyzed. In agreement with findings of Martina et al. (2001), however, we only saw a late inhibitory component when the stimulation electrode was <1 mm from the recorded cell (2 of 8 cells with electrode <1 mm). Paired-pulse stimulation of layer I (20–25 Hz) resulted in mild depression (Fig. 10B; Table 3). Trains of 10 stimuli presented at 20–25 Hz (only frequencies tested) always elicited evoked currents (frequency following), but they rapidly depressed to a steady-state amplitude (Fig. 10E).

DISCUSSION

Unlike previous descriptions of firing properties throughout layer V of the cerebral cortex, which only included RS and BS cells, the present study demonstrates that pyramidal cells in layer V of rat PR also contain a substantial population of LS cells, not found among cortical pyramidal cells outside the PR. The presence of LS

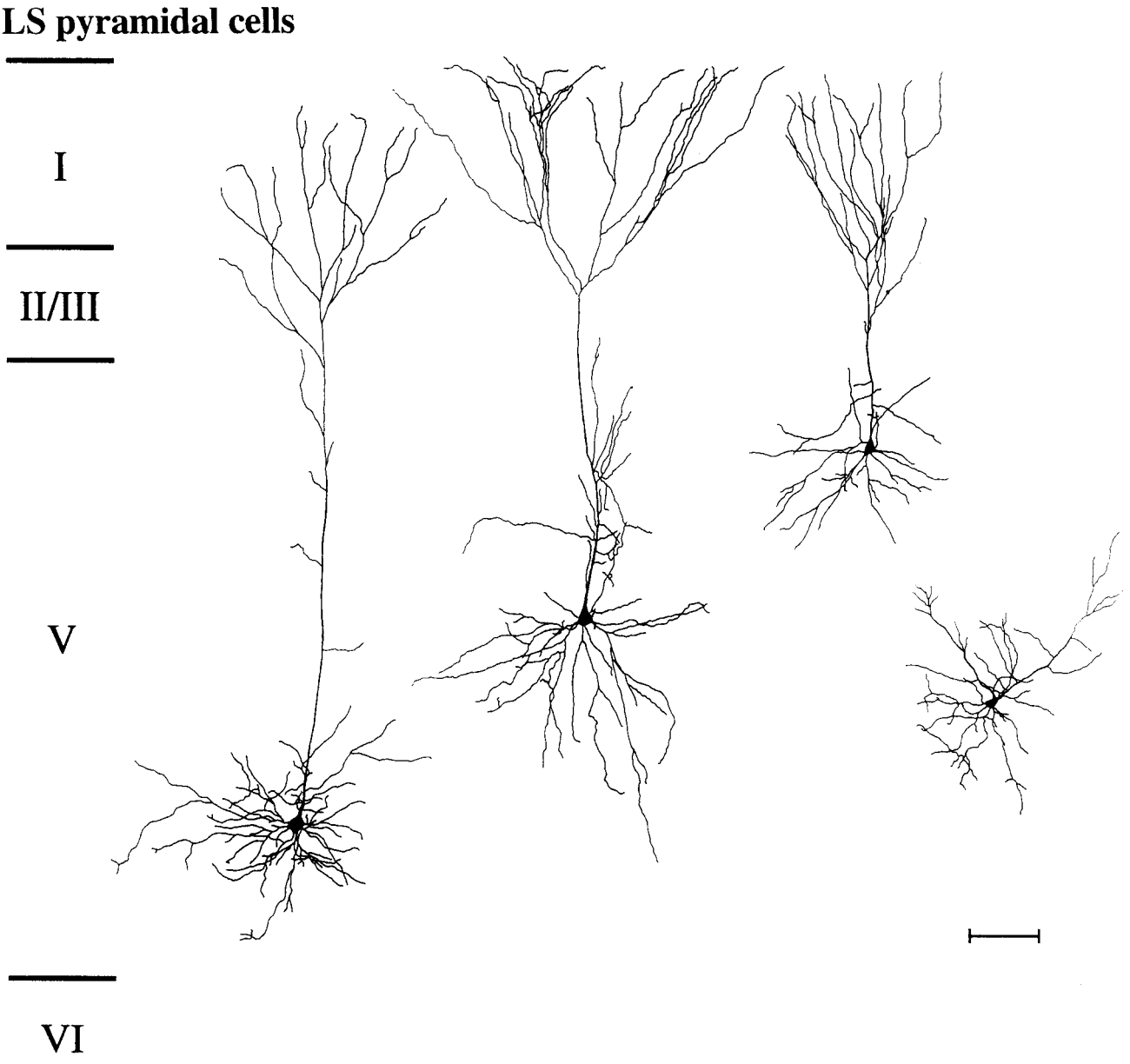

FIGURE 7. Morphology of late-spiking pyramidal neurons in layer V of rat perirhinal cortex. Shown are reconstructions from four biocytin-filled late-spiking cells, illustrating the range of morphologies observed (n = 14). Late-spiking cells were characterized by prominent basilar dendrites and *thin* apical dendrites that ended in a tuft within layer I (left three cells) or, in one case, a bifurcating apical that ended diffusely within layer V (right cell). Although not drawn, LS cells had numerous spines emerging from their basilar and apical dendrites. Cortical layers are indicated by bars and Roman numerals (Scale bar, 100 μm).

cells, along with the long-latency monosynaptically evoked PSCs, suggests that PR is not a region of rapid throughput. On the contrary, PR may be better viewed as a higher-order association cortex with unique processing capabilities that may not exist elsewhere in the cortex.

Three Classes of Pyramidal Neurons in Layer V of Rat Perirhinal Cortex

The presence of LS cells in the present study was surprising because *LS cells have never been reported in layer V of any other cortical region*. Their discharge pattern was dramatically different than that of BS or RS cells, because the latter groups fired shortly after onset of a current step, whereas LS cells exhibited pronounced delays up to 12 s prior to reaching spike threshold. Classifying cells solely on the basis of their individual voltage traces can be ambiguous and subjective. To circumvent this problem and to eliminate some of the subjectivity involved in classifying cells, we constructed ISI-interval number plots (Fig. 2). Each cell type had a characteristic pattern or *fingerprint*, enabling them to be distinguished based on the effect of current intensity on the first ISI and the overall shape of the families of curves. RS and BS cells had upward going curves, indicative of frequency adaptation. With

TABLE 2.

Spontaneous PSCs in Layer V of Rat Perirhinal Cortex[a]

Parameter measured	Mean ± standard error
10/90 rise time (ms)	2.7 ± 0.2
20/80 rise time (ms)	1.8 ± 0.1
Peak amplitude (pA)	14.7 ± 0.9
Decay τ (ms)	16.6 ± 1.2
Holding potential (mV)	−79.8 ± 1.2
Recording time (min)	3.8 ± 0.3
Number of events	662 ± 133
Frequency (Hz)	2.8 ± 0.5

[a]Analyzed data are from 16 pyramidal neurons. PSCs, postsynaptic currents; Decay τ, decay time constant.

increasing current, however, the first ISI decreased rapidly in RS cells but remained constant in BS cells. In contrast, families of ISI-interval number curves in LS cells were, overall, more horizontal, with smaller currents yielding downward going curves (anti-adaptation) and larger currents yielding upward going curves (adaptation). In addition, the first ISI changed in a fairly linear manner, with increased current injection in LS cells. These ISI-interval number plots serve as a graphically simple and objective way to distinguish among the three physiological cell types. With their ability to capture the range of cellular discharge patterns, ISI-interval number plots could be useful for accurately representing different physiological cell classes in computational modeling studies (see Tieu et al., 1999).

Morphologically, BS cells had nontapering, thick primary apical dendrites that terminated in a tuft in layer I, similar to BS pyramidal cells in layer V elsewhere (Chagnac-Amitai et al., 1990; Tseng and Prince, 1993; Franceschetti et al., 1995). Modeling studies suggest that the presence of such a thick primary apical dendrite can increase the tendency of a neuron to burst (Mainen and Sejnowski, 1996). In contrast, RS and LS cells had thin primary apical dendrites and were morphologically indistinguishable from each other, suggesting that differences in ionic conductance distribution or expression rather than dendritic structure are at least partly responsible for the dramatic variations in firing properties among the RS and LS classes of pyramidal neurons in the present study (cf. Mainen and Sejnowski, 1996). Our reconstructions suggest that axons of each cell type ramify within layer V and project toward layer VI and the external capsule (data not shown). However, some LS cells in layer V also sent axons to layers II/III and VI, both of which contain large percentages of LS cells (Faulkner and Brown, 1999; Beggs et al., 2000; McGann et al., 2001).

Comparisons With Late-Spiking Neurons in Other Brain Regions

The only other cortical region where LS cells have been seen is rat frontal cortex, where they were identified as a population of GABAergic, neurogliaform cells, reportedly comprising 11% of nonpyramidal neurons in layer II/III (Kawaguchi, 1995; Kawaguchi and Kubota, 1997). The present study represents the first demonstration of LS cells in layer V anywhere in the cortex, as well as the first demonstration of LS cells in a population of spiny pyramidal neurons in the cortex. Since our LS cells are spiny pyramidal

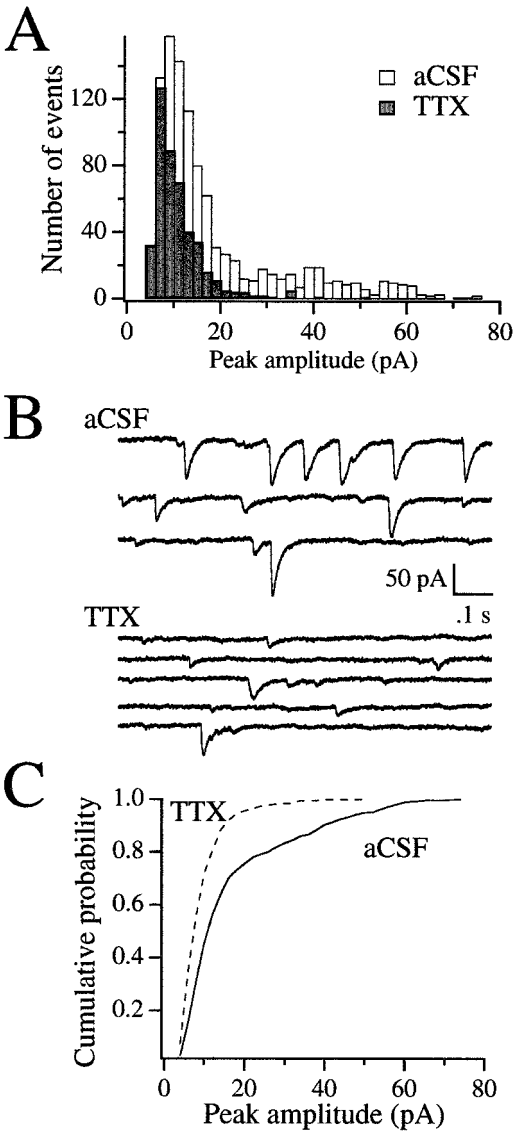

FIGURE 8. Effects of TTX on spontaneous PSCs of pyramidal cells in layer V of rat perirhinal cortex. Data from an RS cell voltage-clamped at −77 mV demonstrates that bath application of 0.5 μM TTX had a dramatic effect on both the frequency and amplitude of spontaneous currents. A: Under control conditions (open bars), the amplitude frequency histogram was positively skewed (1,026 events, frequency 4.3 Hz). Most events were small (mean 18.6 ± 0.4 pA), but 27% of PSCs were larger than 20 pA. In 0.5 μM TTX (shaded bars), the amplitude frequency histogram was still positively skewed (453 events, frequency 1.3 Hz), but only 5% of the currents were larger than 20 pA (mean, 10.7 ± 0.3 pA). B: Individual 1 s sweeps before and after TTX show the dramatic effect of TTX on larger amplitude currents. C: Cumulative probability distributions constructed from the same cell before (solid line) and after (dashed line) bath application of TTX. The substantial shift to the left in the cumulative probability distribution after TTX indicates a statistically significant amplitude reduction (Kolmogorov-Smirnov test, $P < 0.001$).

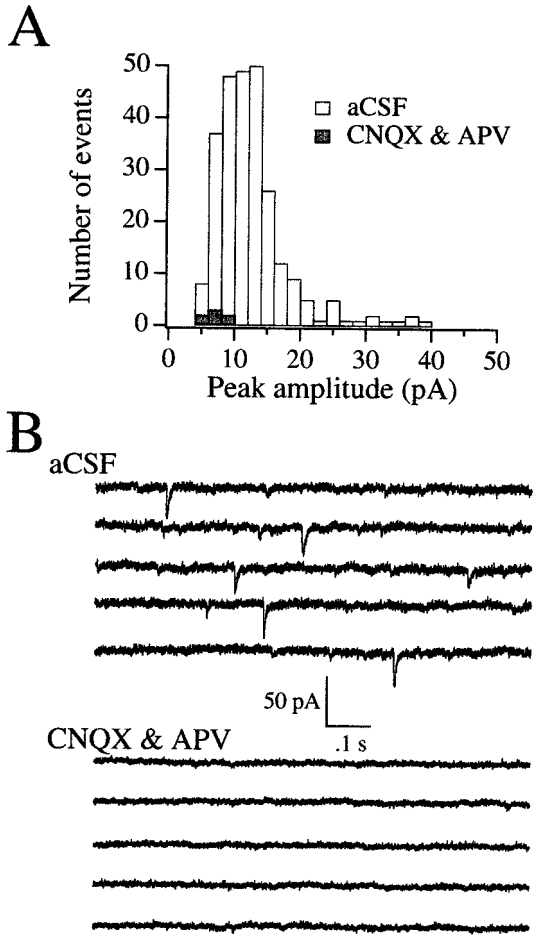

FIGURE 9. Spontaneous PSCs of perirhinal layer V pyramidal neurons recorded near the rest potential are primarily mediated by release of glutamate. A: Amplitude frequency histograms constructed before (open bars, mean PSC amplitude 12.5 ± 0.4 pA, n = 259 events) and after (shaded bars) bath application of a combination of 10 μM CNQX and 50 μM APV indicated that at membrane potentials near rest, greater than 97% of all currents were excitatory. B: Individual 1 s sweeps clearly show the absence of spontaneous activity in the presence of CNQX and APV.

neurons, it is likely that they are excitatory. However, dual-labeling studies will be required to elucidate the excitatory or inhibitory nature of the population of LS cells reported here.

Late-spiking neurons have also been identified in nucleus solitarius type II neurons (Dekin and Getting, 1984, 1987), basolateral amygdala neurons (Washburn and Moises, 1992), superior salivatory parasympathetic neurons (Matsuo and Kang, 1998), hippocampal CA1 neurons (Storm, 1988; Wu and Barish, 1999), neostriatal spiny projection neurons (Nisenbaum et al., 1994; Nisenbaum and Wilson, 1995), and amygdala central nucleus neurons (ACe) (Martina et al., 1999). These various LS cell types are quite different morphologically and physiologically. For example, both nucleus solitarius type II and hippocampal neurons required a strong hyperpolarizing prepulse to show late spiking in response to a depolarizing current step. Some LS neurons in the medial subdivision of ACe are quite different: after the initial delay, they fire a burst of spikes rather than single spikes (Martina et al., 1999). It is unclear whether any of the late-spiking cell types reported elsewhere can show delays as long as those we report here in the perirhinal (up to 12 s), because the investigators used shorter current steps (typically <1 s).

The ionic currents underlying late spiking in perirhinal layer V neurons are currently unknown. Late spiking in hippocampal, neostriatal, and ACe neurons has been suggested to result from a slowly inactivating potassium conductance that is blocked by low concentrations of 4-aminopyridine (4-AP) (Storm, 1988; Nisenbaum and Wilson, 1995; Gabel and Nisenbaum, 1998; Martina et al., 1999). Preliminary data from LS neurons in layers II/III and VI of rat perirhinal indicate that 30 μM 4-AP and 30 nM α-dendrotoxin block late spiking in current-clamp recordings, and that 30 μM 4-AP appears to block a slowly inactivating outward current in voltage-clamp recordings (Moyer et al., 2000).

Spontaneous and Evoked Currents in Layer V Pyramidal Neurons of Rat Perirhinal Cortex

At holding potentials near rest, the spontaneous PSCs we observed were glutamatergic because they were completely blocked by CNQX and APV (Fig. 9). Comparisons with the adjacent amygdala (lateral or basolateral nuclei) indicate that amygdalar neurons receive larger, faster spontaneous PSCs at higher frequencies than PR layer V (Smith and Dudek, 1996; Faulkner and Brown, 1999). Comparisons with the adjacent entorhinal cortex (EC), however, indicate that spontaneous PSCs in the present study are similar in size but occur with higher frequencies than those in EC layers II and IV/V (Berretta and Jones, 1996). Rise times of spontaneous PSCs in EC layer II neurons are faster, whereas rise times in EC layer IV/V neurons are comparable to those of PR layer V (see Table 2 and compare with Berretta and Jones, 1996).

TABLE 3.

Evoked PSCs in Layer V of Rat Perirhinal Cortex[a]

Parameter measured (*n*)	Mean ± standard error
Single pulses (25)	
Onset latency (ms)	9.8 ± 0.7
CV of onset latency	0.07 ± 0.002
10/90 rise time (ms)	4.4 ± 0.6
20/80 rise time (ms)	2.9 ± 0.3
Peak amplitude (pA)	39.5 ± 4.4
Decay τ (ms)	24.3 ± 0.6
Holding potential (mV)	−78.3 ± 0.9
Paired pulses (11)	
Amplitude pulse 1 (ms)	34.1 ± 8.9
Amplitude pulse 2 (ms)	29.3 ± 7.6
Ratio (pulse 1/pulse 2)	0.9 ± 0.1
Holding potential (mV)	−84.4 ± 1.9

[a]Currents were evoked by near-minimal stimulation of layer I (see Methods). CV, coefficient of variation; Decay τ, decay time constant; *n*, number of cells studied.

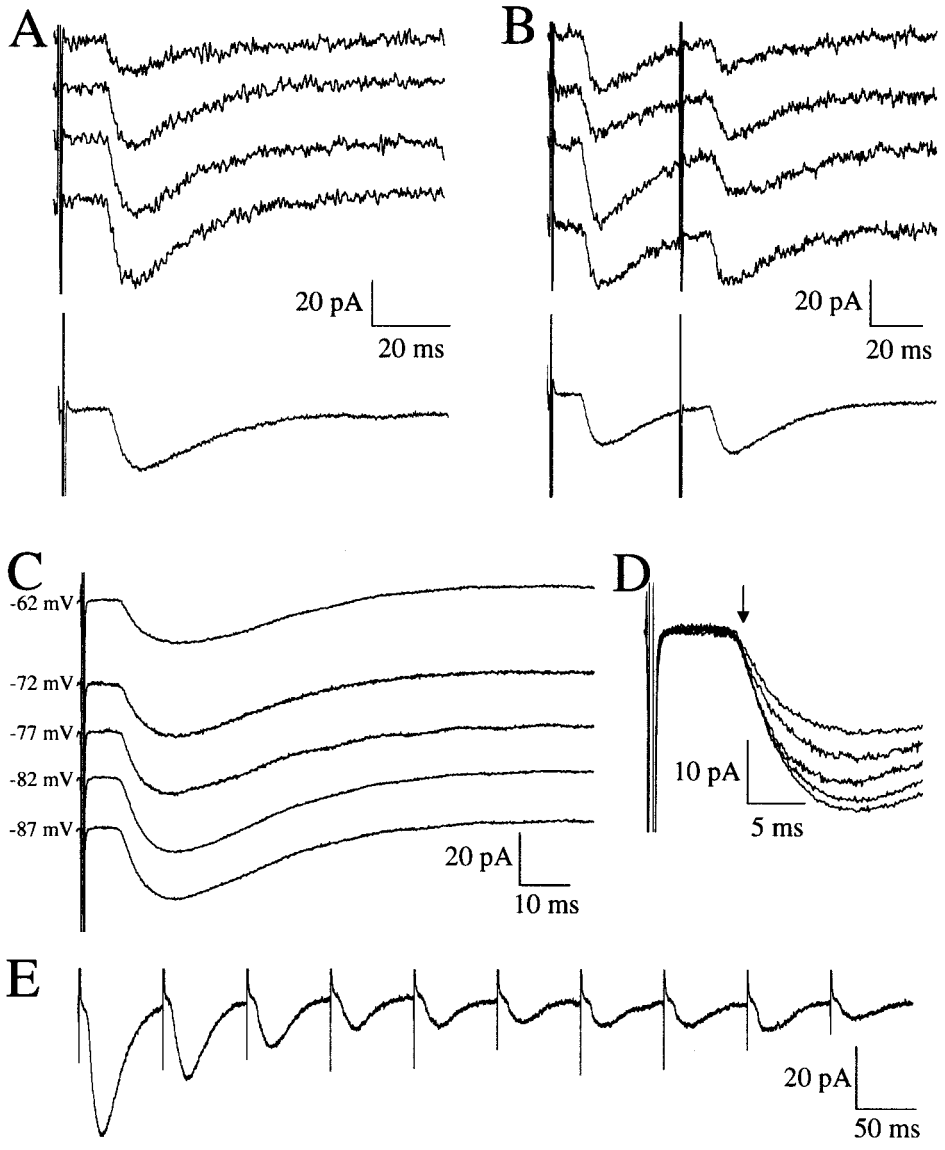

FIGURE 10. Analysis of postsynaptic currents evoked in rat perirhinal layer V pyramidal neurons. A and B: Typical excitatory responses to layer I stimulation. At membrane potentials near rest, purely excitatory evoked PSCs were seen in 6 of 8 cells when the stimulation electrode was <1 mm (C and D) and 17 of 17 cells when it was >1 mm (A and B) from the recorded cell. A: Upper traces are individual currents evoked in response to layer I stimulation. Lower trace shows the average of all 24 evoked responses in an RS cell voltage-clamped at −87 mV. Evoked currents from this cell had a peak amplitude of 17.5 ± 0.8 pA, a 20/80 rise time of 4.4 ± 0.3 ms, and a decay constant of 26.4 ± 2.8 ms. B: Upper traces are individual responses evoked by pairs of stimuli delivered to layer I at an ISI of 50 ms. Lower trace shows the average of all 40 paired-pulse responses. The peak amplitude of the second response was about 10% smaller than the first response. C: Average evoked responses recorded at holding potentials near rest (range, −60 to −90 mV). Neither the onset latency nor the general shape of the evoked response was altered by the membrane potentials used in these experiments. Note the late outward (presumably inhibitory) component in each current trace. D: Overlay of first 25 ms of evoked currents from C indicates that membrane potential had little effect on evoked response amplitude or onset latency (arrow). E: Evoked currents display frequency following. Average of four consecutive evoked PSCs recorded from a different cell (voltage-clamped at −76 mV) in response to 10 stimuli delivered to layer I at 20 Hz. Notice that the amplitude decreased rapidly to a steady state that was maintained throughout the duration of the train.

Bath application of TTX decreased the frequency and amplitude of spontaneous PSCs by a selective reduction of larger-amplitude events (Fig. 8). The effect of TTX can be easily explained if the larger events are multiple quanta evoked by sodium-dependent APs. Similar effects of TTX on both inhibitory and excitatory spontaneous PSCs have been observed in other cell types, including hippocampal, entorhinal, and amygdala neurons (Edwards et al., 1990; Livsey and Vicini, 1992; Arancio et al., 1994; Xiang, 1995; Berretta and Jones, 1996; Cormier and Kelly, 1996; Smith and Dudek, 1996).

Currents evoked by near-minimal stimulation of layer I had larger amplitudes with slower rise and decay times than spontane-

ous PSCs. This is probably due to simultaneous release of multiple quanta from synapses originating remotely relative to the soma. The long latencies of our monosynaptically evoked PSCs suggest activation of small-diameter unmyelinated fibers. Indeed, one hallmark of PR is its relatively low myelin content (Zilles and Wree, 1995), and our estimated conduction velocity of 0.16 m/s is consistent with stimulation of unmyelinated fibers (Berg-Johnsen and Langmoen, 1992; Murakoshi et al., 1993; Lohmann and Rörig, 1994). In addition, all 17 cells where the stimulating electrode was >1 mm from the recorded cell yielded purely excitatory evoked PSCs (Fig. 10A). In contrast, 2 of 8 cells where the stimulating electrode was <1 mm from the recorded cell had evoked PSCs containing a late inhibitory component (Fig. 10C), similar to observations by Martina et al. (2000).

Relationship With Layer V Pyramidal Neurons of Other Cortical Regions

LS cells have not been reported among neurons in layer V of any other cortical region. Since layer V of PR contains three distinct classes of pyramidal neurons, it is unique among cortical layers. In terms of how layer V of PR relates to other cortical regions, several lines of evidence indicate *that layer V of rat PR may be more similar to layer V of EC than to layer V of any other cortical region*. For example, BS cells typically comprise 35–60% of layer V pyramidal cells in other cortices (Connors et al., 1982; Agmon and Connors, 1989; Chagnac-Amitai et al., 1990; Schwindt et al., 1997; Franceschetti et al., 1998). Like layer V of EC (Jones and Heinemann, 1988; Hamm et al., 2000), we observed BS cells among ~9% of PR layer V pyramidal cells (Table 1). Similar to spontaneous PSCs in layer V of EC (Berretta and Jones, 1996), those in PR layer V were small (~15 pA) relative to the adjacent lateral amygdala (Faulkner and Brown, 1999).

Single-unit recordings further support similarities between PR and EC. For example, theta-frequency oscillations of perirhinal neurons correlate highly with EC theta oscillations, and PR neurons lack the ubiquitous neocortical sleep spindles (Collins et al., 1999). Although we did not evaluate subthreshold membrane potential oscillations (MPOs), previous studies demonstrated theta-frequency MPOs in layer V of both EC and PR (Bilkey and Heinemann, 1999; Hamm et al., 2000). Consistent with its role as part of the medial temporal lobe memory system, PR appears to share more features with the adjacent EC than with other cortical regions.

Potential Significance of Late-Spiking Neurons in Rat Perirhinal Cortex

The precise role of LS cells in information processing is currently unknown. Empirical and theoretical studies suggest that cells endowed with LS properties may significantly affect information flow in the network in which they occur. Using the dynamic clamp, Turrigiano et al. (1996) added a slowly inactivating potassium conductance to stomatogastric neurons that were not LS cells. Their data suggest that a potassium conductance with slow kinetics (slowly inactivating and slowly recovering) confers upon neurons a memory of past activation that can last many seconds and depends only on intrinsic properties of the cell. Also, in rat PR layer II/III pyramidal neurons, synaptic stimulation of layer I inputs resulted in pronounced delays in firing, but only in cells that were intrinsically LS cells (Beggs et al., 2000). Thus, in response to trains of synaptic stimulation (20–25 Hz), LS cells fired an AP after a several-second delay, whereas RS cells fired almost immediately. The fact that LS cells show long delays followed by sustained firing with little adaptation could have important ramifications for network function. Through their delayed and sustained firing properties, it has been demonstrated in a computational model that a network containing LS neurons could, theoretically, effectively encode temporal intervals in the range of seconds (Tieu et al., 1999; McGann and Brown, 2000). Alternatively, the relative lack of frequency adaptation in LS cells could also permit a recurrent network to perform a sample-and-hold function.

In summary, layer V of rat PR contains three distinct classes of pyramidal cells based on their firing properties: RS, BS, and LS. The combination of LS cells and long-latency evoked currents suggests that PR is not simply a region of rapid throughput. Such diversity among pyramidal cells within layer V of PR affords unique processing capabilities, not previously observed among pyramidal cells in layer V of any other cortical region. These data support the view that *PR is physiologically unique among cortical regions*.

Acknowledgments

This work was supported by NIH grants RO1 48660 and RO1 50948 to T.H.B., and NINDS postdoctoral fellowship F32 NS09992 to J.R.M. The authors thank A. Szeto, T. Powell, M. Payne, and S. Furtak for assistance with morphology, and J.P. McGann for helpful comments.

REFERENCES

Agmon A, Connors BW. 1989. Repetitive burst-firing neurons in the deep layers of mouse somatosensory cortex. Neurosci Lett 99:137–141.

Arancio O, Korn H, Gulyas A, Freund T, Miles R. 1994. Excitatory synaptic connections onto rat hippocampal inhibitory cells may involve a single transmitter release site. J Physiol (Lond) 481:395–405.

Beggs JM, Moyer JR Jr, McGann JP, Brown TH. 2000. Prolonged synaptic integration in perirhinal cortical neurons. J Neurophysiol 83: 3294–3298.

Berg-Johnsen J, Langmoen IA. 1992. Temperature sensitivity of thin unmyelinated fibers in rat hippocampal cortex. Brain Res 576:319–321.

Berretta N, Jones RSG. 1996. A comparison of spontaneous EPSCs in layer II and layer IV–V neurons of the rat entorhinal cortex in vitro. J Neurophysiol 76:1089–1099.

Bilkey DK, Heinemann U. 1999. Intrinsic theta-frequency membrane potential oscillations in layer III/V perirhinal cortex neurons of the rat. Hippocampus 9:510–518.

Buffalo EA, Reber PJ, Squire LR. 1998. The human perirhinal cortex and recognition memory. Hippocampus 8:330–339.

Burwell RD, Amaral DG. 1998. Perirhinal and postrhinal cortices of the rat: interconnectivity and connections with the entorhinal cortex. J Comp Neurol 391:293–321.

Burwell RD, Witter MP, Amaral DG. 1995. Perirhinal and postrhinal cortices of the rat: a review of the neuroanatomical literature and comparison with findings from the monkey brain. Hippocampus 5:390–408.
Chagnac-Amitai Y, Luhmann HJ, Prince DA. 1990. Burst generating and regular spiking layer 5 pyramidal neurons of rat neocortex have different morphological features. J Comp Neurol 296:598–613.
Collins DR, Lang EJ, Paré D. 1999. Spontaneous activity of the perirhinal cortex in behaving cats. Neuroscience 89:1025–1039.
Connors BW, Gutnick MJ. 1990. Intrinsic firing patterns of diverse neocortical neurons. Trends Neurosci 13:99–104.
Connors BW, Gutnick MJ, Prince DA. 1982. Electrophysiological properties of neocortical neurons in vitro. J Neurophysiol 48:1302–1320.
Cormier RJ, Kelly PT. 1996. Glutamate-induced long-term potentiation enhances spontaneous EPSC amplitude but not frequency. J Neurophysiol 75:1909–1918.
Dekin MS, Getting PA. 1984. Firing pattern of neurons in the nucleus tractus solitarius: modulation by membrane hyperpolarization. Brain Res 324:180–184.
Dekin MS, Getting PA. 1987. In vitro characterization of neurons in the ventral part of the nucleus tractus solitarius. II. Ionic basis for repetitive firing patterns. J Neurophysiol 58:215–229.
deToledo-Morrell L, Sullivan MP, Morrell F, Wilson RS, Bennett DA, Spencer S. 1997. Alzheimer's disease: in vivo detection of differential vulnerability of brain regions. Neurobiol Aging 18:463–468.
Eacott MJ. 1998. Acquisition and retention of visual discrimination learning after ablation of perirhinal cortex in the rat. Psychobiology 26:36–41.
Edwards FA, Konnerth A, Sakmann B. 1990. Quantal analysis of inhibitory synaptic transmission in the dentate gyrus of rat hippocampal slices: a patch-clamp study. J Physiol [Lond] 430:213–249.
Fahy FL, Riches IP, Brown MW. 1993. Neuronal activity related to visual recognition memory: long-term memory and the encoding of recency and familiarity information in the primate anterior and medial inferior temporal and rhinal cortex. Exp Brain Res 96:457–472.
Faulkner B, Brown TH. 1999. Morphology and physiology of neurons in the rat perirhinal-lateral amygdala area. J Comp Neurol 411:613–642.
Franceschetti S, Buzio S, Sancini G, Panzica F, Avanzini G. 1993. Expression of intrinsic bursting properties in neurons of maturing sensorimotor cortex. Neurosci Lett 162:25–28.
Franceschetti S, Guatteo E, Panzica F, Sancini G, Wanke E, Avanzini G. 1995. Ionic mechanisms underlying burst firing in pyramidal neurons: intracellular study of rat sensorimotor cortex. Brain Res 696:127–139.
Franceschetti S, Sancini G, Panzica F, Radici C, Avanzini G. 1998. Postnatal differentiation of firing properties and morphological characteristics in layer V pyramidal neurons of the sensorimotor cortex. Neuroscience 83:1013–1024.
Gabel LA, Nisenbaum ES. 1998. Biophysical characterization and functional consequences of a slowly inactivating potassium current in neostriatal neurons. J Neurophysiol 79:1989–2002.
Hamm BN, Kennedy TE, Alonso A, Amaral DG. 2000. Morphological and electrophysiological characteristics of layer V neurons of the rat medial entorhinal cortex. J Comp Neurol 418:457–472.
Herzog C, Otto T. 1997. Odor-guided fear conditioning. II. Lesions of anterior perirhinal cortex disrupt fear conditioned to the explicit CS but not to the training context. Behav Neurosci 111:1265–1274.
Jones RSG, Heinemann V. 1988. Synaptic and intrinsic responses of medial entorhinal cortical cells in normal and magnesium-free medium "in vitro." J Neurophysiol 59:1476–1496.
Jung H-Y, Mickus T, Spruston N. 1997. Prolonged sodium channel inactivation contributes to dendritic action potential attenuation in hippocampal pyramidal neurons. J Neurosci 17:6639–6646.
Juottonen K, Laakso MP, Insausti R, Lehtovirta M, Pitkänen A, Partanen K, Soininen H. 1998. Volumes of the entorhinal and perirhinal cortices in Alzheimer's disease. Neurobiol Aging 19:15–22.
Kasper EM, Larkman AU, Lübke J, Blakemore C. 1994a. Pyramidal neurons in layer 5 of the rat visual cortex. I. Correlation among cell morphology, intrinsic electrophysiological properties, and axon targets. J Comp Neurol 339:459–474.
Kasper EM, Larkman AU, Lübke J, Blakemore C. 1994b. Pyramidal neurons in layer 5 of the rat visual cortex. II. Development of electrophysiological properties. J Comp Neurol 339:475–494.
Kawaguchi Y. 1995. Physiological subgroups of nonpyramidal cells with specific morphological characteristics in layer II/III of rat frontal cortex. J Neurosci 15:2638–2655.
Kawaguchi Y, Kubota Y. 1997. GABAergic cell subtypes and their synaptic connections in rat frontal cortex. Cereb Cortex 7:476–486.
Keenan CL, Chapman PF, Chang VC, Brown TH. 1988. Videomicroscopy of acute brain slices from amygdala and hippocampus. Brain Res Bull 21:373–383.
Liu P, Bilkey DK. 1998a. Excitotoxic lesions centered on perirhinal cortex produce delay-dependent deficits in a test of spatial memory. Behav Neurosci 112:512–524.
Liu P, Bilkey DK. 1998b. Perirhinal cortex contributions to performance in the Morris water maze. Behav Neurosci 112:304–315.
Livsey CT, Vicini S. 1992. Slower spontaneous excitatory postsynaptic currents in spiny versus aspiny hilar neurons. Neuron 8:745–755.
Lohmann H, Rörig B. 1994. Long-range horizontal connections between supragranular pyramidal cells in the extrastriate visual cortex of the rat. J Comp Neurol 344:543–558.
Mainen ZF, Sejnowski TJ. 1996. Influence of dendritic structure on firing pattern in model neocortical neurons. Nature 382:363–366.
Marchand P, Marmet L. 1983. Binomial smoothing filter: a way to avoid some pitfalls of least-squares polynomial smoothing. Rev Sci Instrum 54:1034–1041.
Martina M, Royer S, Paré D. 1999. Physiological properties of central medial and central lateral amygdala neurons. J Neurophysiol 82:1843–1854.
Martina M, Royer S, Paré J-F, Smith Y, Paré D. 2000. Perirhinal propagation of neocortical inputs. Soc Neurosci Abstr 26:470.
Martina M, Royer, S, Paré D. 2001. Propagation of neocortical inputs in the perirhinal cortex. J Neurosci 21:2878–2888.
Matsuo R, Kang Y. 1998. Two types of parasympathetic preganglionic neurones in the superior salivatory nucleus characterized electrophysiologically in slice preparations of neonatal rats. J Physiol (Lond) 513: 157–170.
McCormick D, Connors B, Lighthall J, Prince D. 1985. Comparative electrophysiology of pyramidal and sparsely spiny stellate neurons in the neocortex. J Neurophysiol 54:782–806.
McGann JP, Brown TH. 2000. Fear conditioning model predicts key temporal aspects of conditioned response production. Psychobiology 28:303–313.
McGann JP, Moyer JR Jr, Brown TH. 2001. Predominance of late-spiking neurons in layer VI of rat perirhinal cortex. J Neurosci 21:4969–4976.
Meunier M, Bachevalier J, Mishkin M, Murray EA. 1993. Effects on visual recognition of combined and separate ablations of the entorhinal and perirhinal cortex in rhesus monkeys. J Neurosci 13:5418–5432.
Moyer JR Jr, Brown TH. 1996. Synaptic currents evoked in layer V perirhinal cortex. Soc Neurosci Abstr 22:1742.
Moyer JR Jr, Brown TH. 1998. Methods for whole-cell recording from visually preselected neurons of perirhinal cortex in brain slices from young and aging rats. J Neurosci Methods 86:35–54.
Moyer JR Jr, Brown TH. 1999. Long latency monosynaptic currents in rat perirhinal cortex. Soc Neurosci Abstr 25:477.
Moyer JR Jr, Szeto A, Brown TH. 1998. Physiology and morphology of perirhinal neurons in adult and aged rat brain slices. Soc Neurosci Abstr 24:1972.
Moyer JR Jr, McGann JP, Brown TH. 2000. Analysis of late spiking in rat perirhinal cortex. Soc Neurosci Abstr 26:1628.
Mumby DG, Pinel JP. 1994. Rhinal cortex lesions and object recognition in rats. Behav Neurosci 108:11–18.
Murakoshi T, Guo J-Z, Ichinose T. 1993. Electrophysiological identification of horizontal synaptic connections in rat visual cortex in vitro. Neurosci Lett 163:211–214.

Naber PA, Witter MP, Lopes da Silva FH. 1999. Perirhinal cortex input to the hippocampus in the rat: evidence for parallel pathways, both direct and indirect. A combined physiological and anatomical study. Eur J Neurosci 11:4119–4133.

Nisenbaum ES, Wilson CJ. 1995. Potassium currents responsible for inward and outward rectification in rat neostriatal spiny projection neurons. J Neurosci 15:4449–4463.

Nisenbaum ES, Xu ZC, Wilson CJ. 1994. Contribution of a slowly inactivating potassium current to the transition to firing of neostriatal spiny projection neurons. J Neurophysiol 71:1174–1189.

Otto T, Eichenbaum H. 1992. Complementary roles of the orbital prefrontal cortex and the perirhinal-entorhinal cortices in an odor-guided delayed-nonmatching-to-sample task. Behav Neurosci 106:762–775.

Otto T, Wolf D, Walsh TJ. 1997. Combined lesions of perirhinal and entorhinal cortex impair rats' performance in two versions of the spatially guided radial-arm maze. Neurobiol Learn Mem 68:21–31.

Paxinos G, Watson C. 1998. The rat brain in stereotaxic coordinates. 3rd ed. San Diego: Academic Press.

Pitkänen A, Pikkarainen M, Nurminen N, Ylinen A. 2000. Reciprocal connections between the amygdala and the hippocampal formation, perirhinal cortex, and postrhinal cortex in rat: a review. Ann NY Acad Sci 911:369–391.

Schwindt P, O'Brien JA, Crill W. 1997. Quantitative analysis of firing properties of pyramidal neurons from layer 5 of rat sensorimotor cortex. J Neurophysiol 77:2484–2498.

Smith BN, Dudek FE. 1996. Amino acid-mediated regulation of spontaneous synaptic activity patterns in the rat basolateral amygdala. J Neurophysiol 76:1958–1966.

Storm JF. 1988. Temporal integration by a slowly inactivating K^+ current in hippocampal neurons. Nature 336:379–381.

Suzuki WA, Eichenbaum, H. 2000. The neurophysiology of memory. Ann NY Acad Sci 911:175–191.

Suzuki WA, Zola-Morgan S, Squire LR, Amaral DG. 1993. Lesions of the perirhinal and parahippocampal cortices in the monkey produce long-lasting memory impairment in the visual and tactual modalities. J Neurosci 13:2430–2451.

Tieu KH, Keidel AL, McGann JP, Faulkner B, Brown TH. 1999. Perirhinal-amygdala circuit-level computational model of temporal encoding in fear conditioning. Psychobiology 27:1–25.

Tseng G-F, Prince DA. 1993. Heterogeneity of rat corticospinal neurons. J Comp Neurol 335:92–108.

Turrigiano GG, Marder E, Abbott LF. 1996. Cellular short-term memory from a slow potassium conductance. J Neurophysiol 75:963–966.

Van Hoesen GW, Solodkin A. 1994. Cellular and systems neuroanatomical changes in Alzheimer's disease. Ann NY Acad Sci 747:12–35.

Washburn MS, Moises HC. 1992. Electrophysiological and morphological properties of rat basolateral amygdaloid neurons *in vitro*. J Neurosci 12:4066–4079.

Wiig KA, Burwell RD. 1998. Memory impairment on a delayed nonmatching-to-position task after lesions of the perirhinal cortex in rat. Behav Neurosci 112:827–838.

Williams SR, Stuart GJ. 1999. Mechanisms and consequences of action potential burst firing in rat neocortical pyramidal neurons. J Physiol (Lond) 521:467—482.

Wu R-L, Barish ME. 1999. Modulation of a slowly inactivating potassium current, I_D, by metabotropic glutamate receptor activation in cultured hippocampal pyramidal neurons. J Neurosci 19:6825–6837.

Xiang Z. 1995. Neurophysiology of mossy fiber synapses in rat hippocampus. Doctoral Dissertation. Yale University, New Haven.

Xiang Z, Brown TH. 1998. Complex synaptic current waveforms evoked in hippocampal pyramidal neurons by extracellular stimulation of dentate gyrus. J Neurophysiol 79:2475–2484.

Young BJ, Otto T, Fox GD, Eichenbaum H. 1997. Memory representation within the parahippocampal region. J Neurosci 17:5183–5195.

Zilles K, Wree A. 1995. Cortex: areal and laminar structure. In: Paxinos G, editor. The rat nervous system. San Diego: Academic Press. p. 649–685.

Zola-Morgan S, Squire LR, Clower RP, Rempel NL. 1993. Damage to the perirhinal cortex exacerbates memory impairment following lesions to the hippocampal formation. J Neurosci 13:251–265.